



Iranian Research Organization
for Science and Technology
(IROST)



Adsorption of fluoride ions from aqueous solution by rice husk based nanocellulose

Savita Sihag, Jitender Pal*

Department of Environmental Science and Engineering, Guru Jambheshwar University of Science and Technology, Hisar-125001 (Haryana), India

ARTICLE INFO

Document Type:
Research Paper

Article history:
Received 14 November 2022
Received in revised form
9 August 2023
Accepted 14 August 2023

Keywords:
Nanocellulose
Characterization
Batch Study
Adsorption
Defluoridation

ABSTRACT

Synthesis of nanocellulose using crop residue rice husk is an innovative method. Morphological and structural characterizations of nanocellulose were analyzed. The rice husk based nanocellulose had a particle height of 5.7 nm and a crystallinity index of 70%. Raw rice husk comprises 35% cellulose, 22% hemicellulose, 19.1% lignin, and 20% ash. Defluoridation of water samples is an imperious provocation for the advancement of society. According to World Health Organisation (WHO) guidelines, a fluoride concentration of more than 1.5 milligrams per litre leads to dental problems and bone deficiency. The appropriate defluoridation practice was selected to avoid these problems. Cost-effective nanocellulose from rice husk was used as an adsorbent to purify a fluoride-rich aqueous solution in batch experiments on a lab scale. Response of dose, temperature, time, pH, and initial ion concentration on adsorption capacity and removal efficiency were deliberated. In batch experiments, the highest removal efficiency of fluoride from aqueous solution was 74% at a 120 min time, 2 mg/l initial ion concentration, 30 °C temp, 0.9 g adsorbent dose at pH 2. According to WHO standards, fluoride concentrations above 1.5 mg/l cause tooth and bone insufficiency. Regeneration showed that the adsorbent was cost-effective and reusable. Two, three, and four-parameter isotherm models were applied to the experimental data. The Freundlich, Langmuir, Temkin, Redlich-Peterson, and Baudu isotherm models and the pseudo-second-order kinetic and intra-particle diffusion models best fit the data. The studied thermodynamic constraints showed the physical adsorption of fluoride.

1. Introduction

Eight hundred million individuals have been exposed to fluoride-contaminated water on a global scale. Water is vital to living organisms.

Water contains numerous contaminants, including fluoride, mercury, lead, zinc, etc., and fluoride must be treated as the primary concern. Fluoride is present in the earth's crust in more than twenty-

*Corresponding author Tel.: +91-1662-263327

E-mail: j_pal2k1@yahoo.com

DOI:10.22104/AET.2023.5963.1643

COPYRIGHTS: ©2023 Advances in Environmental Technology (AET). This article is an open access article distributed under the terms and conditions of the Creative Commons Attribution 4.0 International (CC BY 4.0) (<https://creativecommons.org/licenses/by/4.0/>)

five countries, penetrating the groundwater. Fluoride ions have a significant impact on densely populated areas in India. The World Health Organisation and Environmental Protection Agency's guiding principle is that the concentration of fluoride ions should be less than 1.5 milligrams per litre. Concentrations over 1.5 mg/l cause tooth enamel cavities, paralysis, gene mutation, bone damage, and RNA/DNA synthesis. Eighty percent of water-related disorders and sixty-five percent of endemic fluorosis are caused by fluoride ingestion, according to the WHO [1-3]. Fluoride contamination of groundwater by anthropogenic and natural processes is one of the world's biggest environmental issues [4]. Rainfall causes the fluoride in the minerals to percolate naturally. Typical industrial applications of fluoride, such as aluminum, fertilizer, semiconductor, and nuclear industries, result in substantial quantities of fluoride-containing effluent [5-7]. Fluoride concentration in groundwater used for drinking purposes exceeds the permissible range in a number of countries, including India, Mexico, China, and the United States [8]. It is necessary to defluoridate excessively fluoride-concentrated drinking water. Numerous techniques, including electro dialysis [9], precipitation [10], reverse osmosis [11], ion exchange [12], and adsorption [13], have been used to defluoridate water. The adsorption process was chosen for removing fluoride from water because of its simplicity, greater efficacy, environmental friendliness, and low cost [14,15]. Several adsorbents, including nanocellulose synthesized from crop residue, activated clay, carbonaceous materials, titanium-rich bauxite, activated carbon, natural polymers in modified form, and zeolites, have been utilized for defluoridation [8,16,17]. Adsorbent excellence is determined by its beneficial cost ratio. Cellulose is a renewable and efficient polymer on earth. Cellulose is used in the synthesis of a cost-effective adsorbent for fluoride removal [18]. Rice husk is composed of fibre, protein, and oxygen functionality (hydroxyl, carboxyl, etc.) [19]. In recent years, adsorption has become a common technique for producing adsorbent materials with chemical functionality and a large surface area. This method is dependent on pH, contact time, and temperature, and it incorporates both chemical

and physical connections (oxygen's functionality with hazardous ions and molecules' agglomeration on the surface by physical forces) [20]. The objective of this research was to assess the effectiveness of nanocellulose synthesized from rice husk for removing fluoride from water.

2. Material and methods

2.1. Determination of lignocellulosic composition

The lignocellulose composition of the raw rice husk was determined by the Georing and Van Soest method (1970) given below [21].

2.1.1. Estimation of cellulose and lignin content

1 g of powdered rice husk (W) was refluxed with 100 ml of acid detergent solution for one hour. The mixture was filtered using a Gooch crucible G-1; the residue was initially washed using hot distilled water and then with acetone until it became colourless. The crucible with acid detergent fibre (ADF) was oven dried and weighed (W_1). Lignin was removed from the ADF by mild oxidation using 25 ml of potassium permanganate solution for 1.5 hours. Excessive potassium permanganate solution was removed by demineralizing solution until the fibre became white. The residue fibre was washed with ethanol and acetone. The weight loss was estimated as lignin content (W_2). The residue was burned at 500°C, and the weight loss was obtained as cellulose (W_3).

The lignin and cellulose were calculated using Equations (1) and (2) given below:

$$\text{Lignin (\%)} = \frac{W_1 - W_2}{W} * 100 \quad (1)$$

$$\text{Cellulose (\%)} = \frac{W_2 - W_3}{W} * 100 \quad (2)$$

2.2.2. Estimation of hemicellulose content

100 ml of a neutral detergent solution was put into a reflux condenser having 1 g of dried rice husk, and then 2-4 drops of octanol were added to prevent foam production. The mixture of added chemicals and rice husk was refluxed for 60 min and filtered. The obtained residue was washed with deionized water, then, it was again washed with 25 ml acetone and 25 ml ethanol. The washed residue was oven dried to obtain the dry weight (W_4). The obtained dried residue was put into the reflux

condenser, and 100 ml of acid detergent solution and 2-4 drops of octanol were added. It was boiled for 50 min; the residue was washed using the same procedure discussed above. The washed residue was oven dried to obtain the dry weight (W_5). The hemicellulose was calculated using Equation (3) given below:

$$\text{Hemicellulose (\%)} = \frac{W_4 - W_5}{W} * 100 \quad (3)$$

2.2.3. Determination of ash content

The ash content was calculated by placing the dried rice husk in a muffle furnace at 500°C for 12 hours to burn the carbon content. The ash content was calculated using Equation (4) given below:

$$\text{Ash Content (\%)} = \frac{W_2 - W}{W_1} * 100 \quad (4)$$

where, W = Ignited weight of dish (gram), W_1 = Initial weight of the dried sample (gram), W_2 = Sample weight along with dish weight after removal from the furnace (gram).

2.2. Synthesis of nanocellulose

The rice husk sample was collected from the rural areas of Hisar City. The collected sample was washed, dried, ground, and sieved. The powdered

sample was oven dried at 40 °C and stored in an airtight container. The synthesis of nanocellulose from rice husk using multi-step treatments is shown in Figure 1. Rice husk was given an alkaline treatment using 5% w/v sodium hydroxide on a magnetic stirrer for two hrs at 70 °C to remove the hemicellulose and lignin. The bleaching of the alkali-treated rice husk was carried out with 6% (w/v) sodium chlorite solution at 60°C to obtain white fibres, and the maximum amount of lignin was removed. Acid hydrolysis of the bleached rice husk fibres was used to obtain cellulose; the fibres were dipped in a 25% (w/v) concentrated sulphuric acid solution and heated at 40 °C for 45 min on a hot plate. The fibres were centrifuged at 5000 rpm for 10 min until the solution pH became neutral. The suspension was sonicated at 60 °C for 45 min, and magnetic stirring was repeated 3-4 times. The acid hydrolyzed fibre was cryo-crushed using liquid nitrogen to freeze the cellulose fibres. Ice crystal pressure was applied to the cell walls, and the high shear forces were functional. The cell walls were ruptured, and nanocellulose was obtained, as shown in Figure 1. Analytical grade chemicals were used throughout the processes. Double-deionized water was utilized in all experimentations.

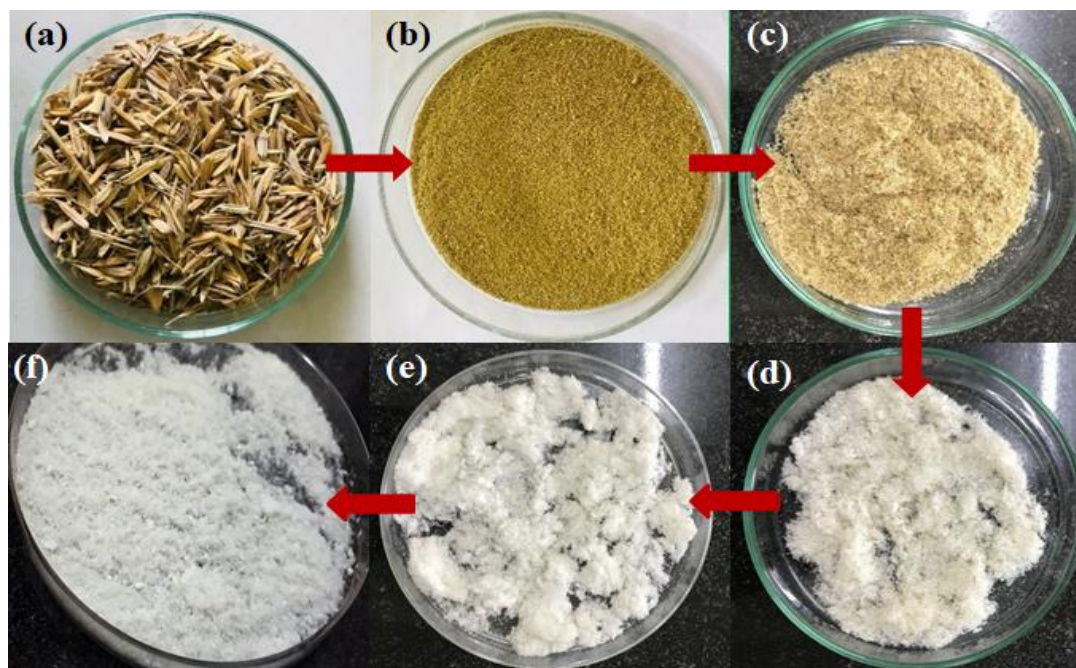


Fig. 1. Synthesis of nanocellulose a) Raw rice husk, b) Powdered rice husk, c) Alkali treated, d) After bleaching, e) After acid hydrolysis, and f) Nanocellulose.

2.3. Characterization

2.3.1. Fourier Transform Infrared Spectroscopy (FTIR)

FTIR analysis was performed for the raw rice husk, alkali treated, bleached treated, acid hydrolysis, and the nanocellulose via a Perkin-Elmer Fourier Transform Infrared instrument using wavelengths ranging from 4000-500 cm^{-1} . The samples were finely ground, and the sample to be analyzed was assorted with *potassium bromide (KBr)*.

2.3.2. X-Ray Diffraction (XRD)

Samples of the raw rice husk, alkaline treated, bleached treated, acid hydrolysis, and the nanocellulose were X-rayed using an X-ray diffractometer with a monochromatic $\text{CuK}\alpha$ energy basis, having 2θ ranges between 10° - 50° , with a phase of 0.04 and a six min. scanning time. In the fine powdered form, samples are placed on the sample holder and uniformly distributed to obtain proper X-ray contact. The crystallinity index was calculated using the Segal formula (5) shown below:

$$\text{CrI (\%)} = I_{002} - \frac{I_{\text{am}}}{I_{002}} * 100 \quad (5)$$

where, the diffraction max intensity of (002) peak of the lattice is I_{002} , then the amorphous cellulose intensity value is I_{am} . The amorphous region scattered energy is restrained at the diffraction angle, i.e., (2θ - 18°), and the diffraction angle around 2θ - 22° is located at the diffraction peak.

2.3.3. Atomic force microscopy (AFM)

The surface topographical structure of the nanocellulose was analysed by a multimode scanning probe microscope (Bruker) AFM. Cantilevers made up of silicon with a frequency of 230 kilo Hertz are utilized at room temperature for imaging in a tapping manner. The rate of scanning was 1.5 Hertz.

2.3.4. Zeta potential

The charge on the nanocellulose surface in suspension was analyzed by the dynamic light scattering method via the Malvern Zeta sizer Nano-ZS90 at 25C with 0.8872 cP viscosity.

2.3.5. Thermogravimetric analysis (TGA)

The thermal stability of the nanocellulose was characterized using METTLER. A 5mg specimen was heated at 500°C to 850°C at the rate of $50^\circ\text{C}/\text{min}$. Thermal stability was observed as the weight loss rate as a function of time.

2.3.6. Field Emission Scanning Electron Microscopy (FESEM)

The morphological structure of raw rice husk powder and nanocellulose was determined by FESEM (Merlin Compact, Carl Zeiss) with a 30 kV acceleration voltage of 1.6 nm at 1 kV. The gold coating was done to the sample by an "ion sputter coater" before analysis.

2.3.7. Transmission Electron Microscopy (TEM)

The extracted nanocellulose was analyzed by TEM using the Tecnai G² 20 (FEI) S-Twin transmission electron microscope with an acceleration voltage of 200 kV. Sample ion milling was done to expose the pristine surface of the sample for imaging; then, the sample was put on a grid coated with copper. The grid was stained using uranyl acetate solution, and after that, the grid was allowed to dry at room temperature.

2.4. Fluoride solution

By dissolving 221 mg of anhydrous sodium fluoride in one litre of double deionized water, the fluoride stock media was ready. The standard solution of fluoride was prepared by diluting hundred ml of the stock solution into one litre of double deionized water. This one ml solution contains 0.1 mg of fluoride. All the experiments were performed on an aqueous solution.

2.5. Equipment

Using the standard method, the Eutech ION 2700 Fluoride Meter was used to determine the fluoride ions in the aqueous solution.

2.6. Fluoride removal by adsorption

The optimal parameters response, like pH contact time, initial ion concentration, temperature, and sorbent dosage, determine the extent of sorption and its proper applicability. Sorption studies were performed in batch trials, yielding steady data as well as an adsorption rate on varied pH (2, 3, 4, 5, 6, 7, 8, 9, 10), contact times (20, 30, 40, 50, 60, 70,

80, 90, 120, 150, 180 min), adsorbent dosages (0.1, 0.2, 0.3, 0.4, 0.5, 0.6, 0.7, 0.8, 0.9, 1.0 g), temperature (10, 20, 30, 40, 50, 60°C), and ion concentrations (2, 5, 8, 10, 13, 15 mg/l). One parameter was varied, and the other remained constant. Experiments were performed using a suitable dose of adsorbent and with the known concentration of fluoride ion having a 50 ml solution. The rate of stirring was 150 rpm for all the experiments done. Double-deionized water was used in all the experiments. The removal efficiency (%) and adsorption capacity of nanocellulose (mg/g) were computed using Equations (6) and (7):

$$\text{Removal efficiency (\%)} = \frac{C_o - C_f}{C_o} * 100 \quad (6)$$

$$\begin{aligned} \text{The adsorption capacity of nanocellulose (q}_e\text{)} \\ = \frac{C_o - C_e}{m} * V \end{aligned} \quad (7)$$

where, C_o (mg/l) is the initial concentration, C_f (mg/l) is the residual concentration, C_e (mg/l) is fluoride concentration at equilibrium, q_e (mg/g) is the fluoride ions sorbed (g) nanocellulose at steady state, V (L) is the volume of an aqueous solution of fluoride, and m (g) is mass of nanocellulose.

2.7. Kinetics, Isotherm Models, and Thermodynamics

Using varied contact times and time square root, pseudo-first-order and pseudo-second-order kinetics studies and an intra-particle diffusion model, respectively, were developed using the adsorption data; the adsorption isotherms were obtained based on the adsorption data from the varied initial fluoride ion concentration. The order and rate of reaction were obtained from the slope and intercept, respectively. The Freundlich, Langmuir, Temkin, Redlich-Peterson, and Baudu isotherm models were applied by plotting curvatures based on the obtained adsorption data, and the best-fitted models of the experimental data were determined. A thermodynamics study on a varied range of temperature adsorption data was

used to determine the effect of temperature on adsorption. Entropy, enthalpy, and Gibbs free energy were deliberated using respective formulas.

2.8. Adsorbent Regeneration

The regeneration adsorption experiments were performed with optimum conditions analyzed during batch experiments (pH of 2, adsorbent dose of 0.9 g, contact time of 120 min, temperature of 30°C, and initial ion concentration of 2 mg/l), and similar conditions were applied for successive cycles. After each cycle, the adsorbent was treated using a desorption solution of sodium hydroxide (0.1M-0.7M) at 150 rpm for two hours, filtered, washed with distilled water, dried, and reused in the next cycle. The efficacy of fluoride ions was intended using Equation (8):

$$\begin{aligned} \text{Regeneration Efficiency (\%)} \\ = \frac{\text{Concentration of fluoride released}}{\text{Initial concentration of sorbed fluoride}} * 100 \end{aligned} \quad (8)$$

3. Results and discussion

3.1. Determination of lignocellulosic composition

The lignocellulosic composition of the raw rice husk contains cellulose (35%), hemicellulose (22%), lignin (19.1%), and ash content (20%), as shown in Table1. Different research study results are compared with the present study. The compositional differences in lignocellulosic composition occurred because of the selected rice crops and ecological conditions.

3.2. Characterization of synthesized nanocellulose

3.2.1. Fourier Transform Infrared Spectroscopy (FTIR)

The peaks at 3420-3440 cm^{-1} in all the analyzed samples showed the stretching vibration of the O-H in the molecules of cellulose, and similar results were observed [24]. The peaks between 1641-1650 cm^{-1} showed O-H bending of liquid adsorption, and similar results were observed [25]. Peaks at 1442 and 1641 cm^{-1} showed that cellulose was present in the prepared material.

Table 1. Composition of cellulose, hemicellulose, lignin, and ash content in rice husk.

Cellulose (%)	Hemicellulose (%)	Lignin (%)	Ash content (%)	References
38.6	20.2	19.8	20.3	[22]
32.67	31.38	18.81	11.88	[23]
35	22	19.1	20	Present study

Peaks at 1160-1170 cm^{-1} showed CC ring-stretching and ether linkages of C-O-C glycosidic, and similar results were observed [25]. Peaks at 1052 cm^{-1} , 1168 cm^{-1} , 1165 cm^{-1} , 1111 cm^{-1} , 1056 cm^{-1} , 1055 cm^{-1} , 1054 cm^{-1} , and 1053 cm^{-1} contributed to cellulose, the stretching C-O, bending vibration of O-H, and deformation vibration of C-H. The peak at 897 cm^{-1} in the alkali-treated, bleached-treated, acid hydrolysis, and nanocellulose showed the stretching vibration C-O-C of the pyranose ring and the linkages of glycosidic within cellulose by the glucose units, as shown in Figure 2(a), and similar results were observed [26].

3.2.2. X-Ray Diffraction (XRD)

Degree of crystallinity by X-Ray Diffraction (XRD)
XRD analysis was used for observing the crystalline structure of the raw rice husk, alkali treated, bleached fibres, acid hydrolysis, and nanocellulose, as shown in Figure 2(b). Peaks were shown at 2theta- 16°, 22°, 26° (raw rice husk), and 35°. 2theta- 16° and 22° are the main peaks that showed the orderly arranged crystalline structure, and similar results were observed [24,25]. Crystallinity can be stated as the crystalline region diffraction divided by the total diffraction of the specimen observed [27]. The crystalline index (%) of the treated samples was determined and is illustrated in Table 2.

Table 2. Crystallinity index (Crl%).

Sample (Rice Husk)	Crl (%)
Raw Rice husk	32%
Alkaline treated	43%
Bleached fibres	60%
Acid hydrolysed	66%
Nanocellulose	70%

The crystallinity index of the raw rice husk was 32%, which increased to 70% in the nanocellulose. The progressively increasing crystallinity occurred due to the exclusion of lignin and hemicellulose amorphous provinces throughout the alkaline process, resulting in crystalline regions rearrangement. In the bleaching treatment, the remaining amorphous components were also removed. While in acid hydrolysis, the amorphous domains of cellulose penetration of hydronium ions showed hydrolytic cleavage of the glycosidic bonds that release individual crystals, and similar results were observed [28]. As the crystallinity increased, the strength, stiffness, and then rigidity also

improved. The maximum surge in the crystalline structure was observed next to the acid hydrolysis process, and similar results were observed [29,30].

3.2.3. Atomic Force Microscopy (AFM)

The nanocellulose was analyzed by Atomic Force Microscopy (AFM) to determine its topographical structure. Figure 2(c) illustrates the 3D image of a nanocellulose surface with a conical shape structure on the smoother surface as well as a particle height of 5.7 nm with a mean roughness of 103.1 nm determined using Gwyddion software. The nanocellulose showed a particle height of 5.7 nm due to the homogeneity of the analyzed sample. It occurred because of the exclusion of pectic polysaccharides that created definite nanocrystallites of cellulose, and similar results were observed [31].

3.2.4. Zeta potential

Zeta potential indicated that the nanocellulose had a mean zeta potential value of -23.1 mV. The negative charge was observed on the nanocellulose surface, shown in Figure 2(d). The synthesized nanocellulose had moderate stability.

3.2.5. Thermogravimetric analysis (TGA)

The thermostability of nanocellulose was determined by TGA, as shown in Figure 2(e) Because of the difference that occurred in the chemical assemblies amongst the cellulose, lignin, and hemicellulose, decomposition was observed over a varied range of temperatures. The initial small amount of loss in weight (0.39%) was observed due to the evaporation of moisture that was loosely bound to the nanocellulose surface at a temperature of 25-160°C. Initial decomposition was observed due to cellulosic decomposition of the glycosylic units, depolymerization, and dehydration, and similar results were observed [32]. Secondly, weight loss was observed (5.21%) at a temperature range of 200-360°C. Thirdly, weight loss was observed (0.62%) at temperatures of 360-520°C. Finally, rapid degradation in weight loss was observed (0.41%) after a temperature of 520°C. Nanocellulose degradation started around 360 °C and continued up to 880°C, and similar results were observed [33]. The fibre's weight prevailing after heating 400°C was of carbon content [34].

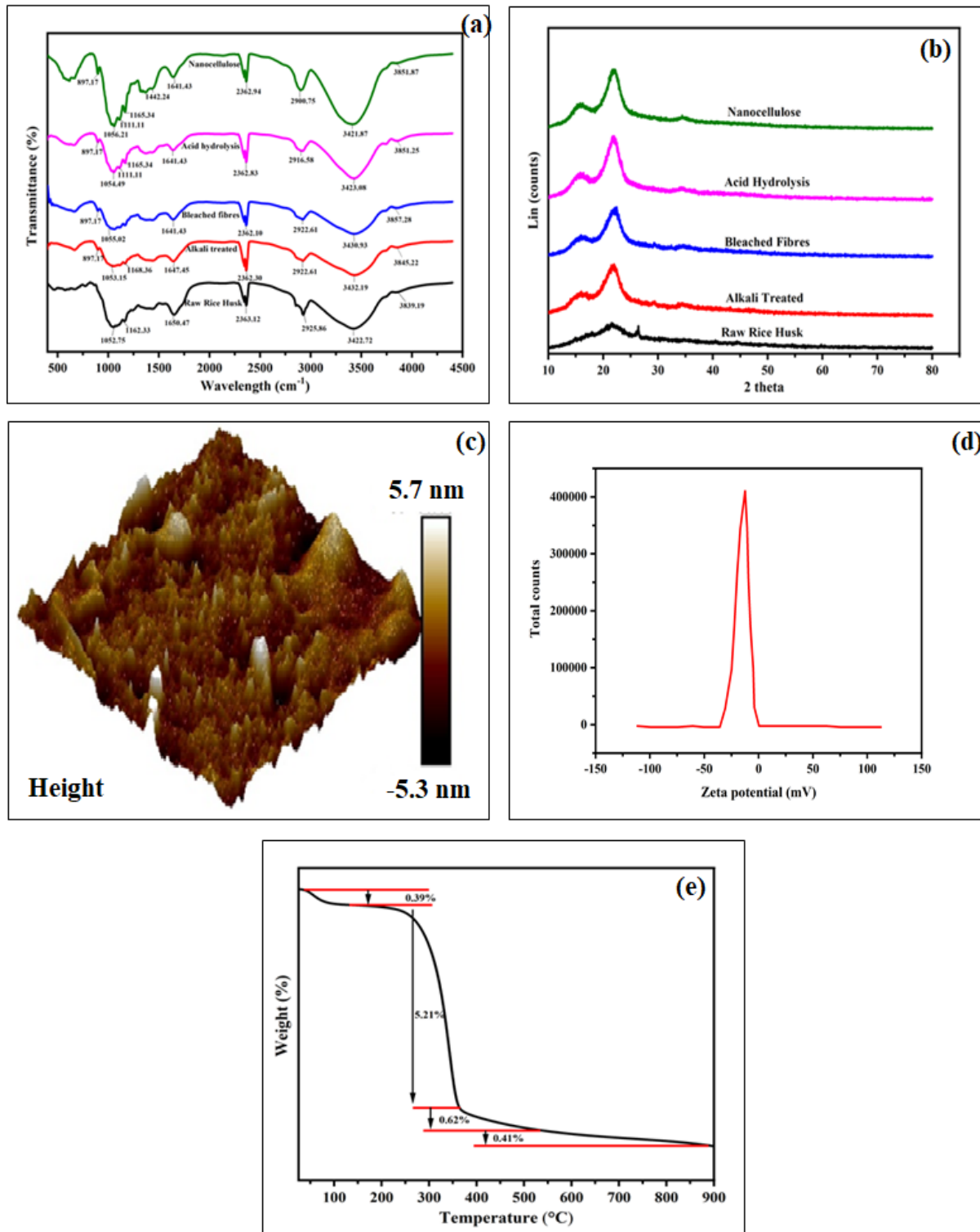


Fig.2.Characterization of nanocellulose a) FTIR, b) XRD, c) AFM, d) Zeta potential, and e) TGA.

3.2.6. Field Emission Scanning Electron Microscopy (FESEM)

FESEM analysis illustrates the morphological structure of raw rice husk and nanocellulose, as shown in Figures 3(a) and (b), respectively. The raw rice husk has a disordered structure. After the

chemical treatments, nanocellulose had a smooth regular structure showing straight fibres connected, obtaining a homogeneous structure. These obtained straight fibres have wide applicability.

3.2.7. Transmission Electron Microscopy (TEM)

TEM micrographs of the nanocellulose divulge the homogeneous structure and the nanometric extents of the nanocellulose. The extracted nanocellulose had a spherical shape structure connected to the forming clusters, as shown in Figure 3(c). The size and shape of the nanocellulose affected the properties, such as stability, optical characteristics, and rheology, and the spherical shape structure of nanocellulose regulated the application of nanocellulose. The histogram showed the diameter of the nanocellulose at 17-24 nm had a 1% count, 24-40 nm had a 3% count, 40-48 nm had a 2% count, and 48-55 nm had a 1% count, as shown in Figure 3(d). A maximum of 3% count occurred at the 24-40 nm diameter range.

3.3. Adsorption

3.3.1. Response of pH

In batch studies, the fluoride intake capacity on nanocellulose was examined at various initial ion concentrations (2, 5, 8, 10, 13, and 15 mg/l) and varying pH (2, 3, 4, 5, 6, 7, 8, 9, and 10) in 120 min using a 0.9g dose at 30 °C. Defluoridation was the highest (50%) at pH 2 and reduced upto 5% at pH 10, as shown in Figure 4(a). The result demonstrated that removal decreased as the pH increased. These results indicated that it occurred as a result of negative charge ions of fluoride being neutralized at the nanocellulose surface by elevated H⁺ ions in the tested aqueous solution, and similar results were determined on the adsorbent of the leaf [35].

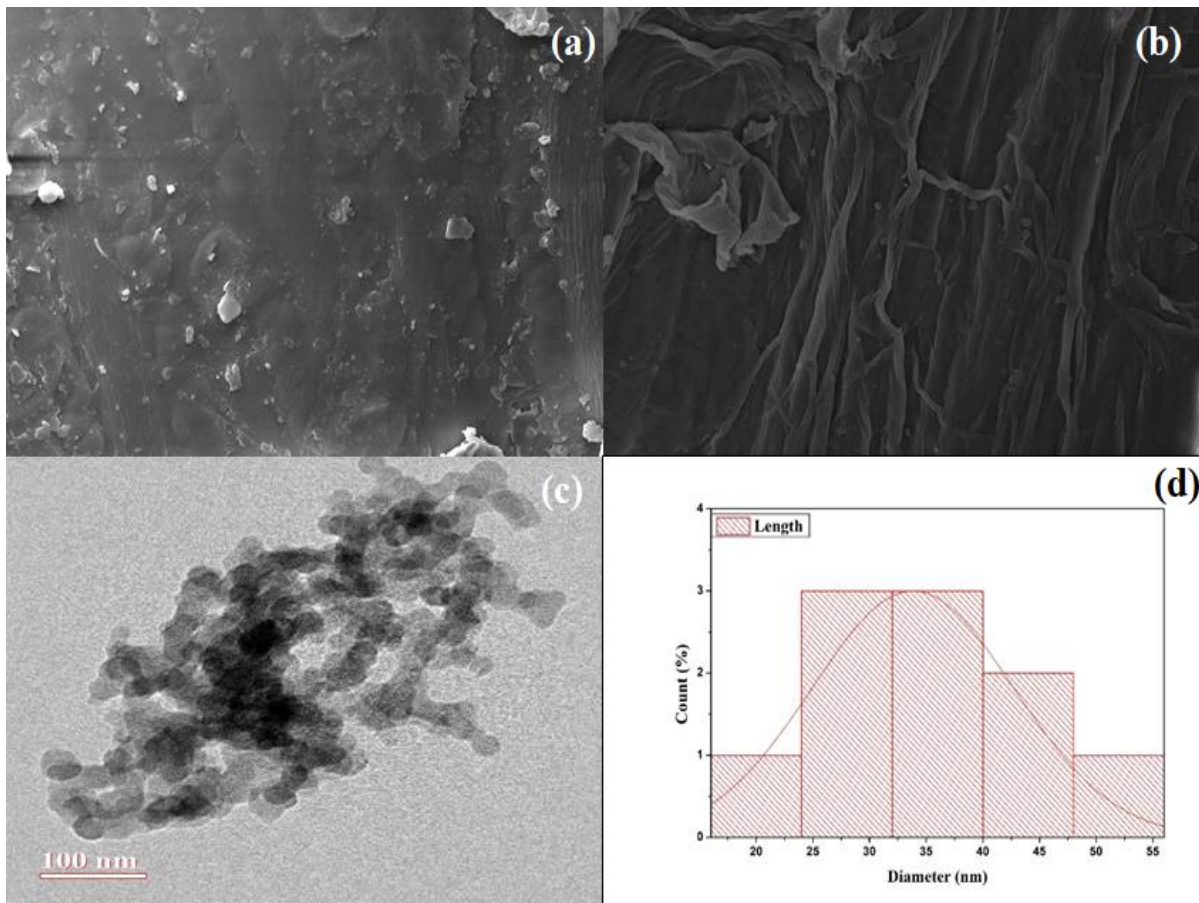


Fig.3. Characterization of nanocellulose a) FESEM, raw rice husk, b) nanocellulose, c) TEM, and d) histogram of TEM.

3.3.2. Response of adsorbent dose

Different initial ion concentrations (2, 5, 8, 10, 13, and 15 mg/l) were used in batch experiments to determine the fluoride adsorption capacity of the

nanocellulose by increasing the adsorbent dose from 0.1 to 1.0 g in aqueous solution at 30°C, 120 min, and pH 2. The highest defluoridation of 60% was observed at 2 mg/l using a 0.9 g dose. The removal of fluoride ions increased as the adsorbent

dose increased up to 0.9 g, as shown in Figure 4(b). The results indicated that as the nanocellulose dose increased, the amount of fluoride removed also increased. Fluoride removal efficacy rose as the dose increased due to the greater surface area and the large number of fluoride adsorbing sites available; similar results were obtained on rice husk adsorbent [36].

3.3.3. Response of contact time

In batch experiments at varied initial ion concentrations (2, 5, 8, 10, 13, and 15 mg/l), by varying contact time (20-180 min) using a 0.9 g dose, pH of 2, and a temperature of 30 °C, the fluoride sorption capacity of the nanocellulose was evaluated. The maximum fluoride removal (74%) was observed at a low concentration of fluoride (2 mg/l) at a constant pH of 2, a dose of 0.9 g, a temperature of 30 °C, and a time of 120 min; after that, the removal was observed steady upto 180 min, as shown in Figure 4(c). As the contact time increased, fluoride removal also increased to a certain range, after which the uptake reached equilibrium due to the non-availability of the sites on the nanocellulose to the fluoride ions; similar results were determined on the rice husk adsorbent [36]. Changes in adsorption capacity might occur because most of the fluoride ion concentration was high and most of the adsorbent sites were open. Fluoride ions uptake on the nanocellulose was decreased because the available active sites were reduced; similar results were determined by [37,38].

3.3.4. Response of temperature

In batch experiments at varied initial ion concentrations (2, 5, 8, 10, 13, 15 mg/l), by varying temperatures (10-60 °C) using a 0.9 g dose, pH of 2,

and a contact time of 120 min, the fluoride adsorption capacity of the nanocellulose was observed. The highest defluoridation (68%) was observed at 2 mg/l, 0.9 g dose, 120 min at pH 2, as shown in Figure 4(d). Due to the attractive force between fluoride ions, it was concluded that the maximal fluoride removal occurred at 30 °C, after which it began to decrease and reached equilibrium as the temperature rose further; similar results were observed in calcium-impregnated silica collective with titanium dioxide [38]. From 26.85 °C to 46.65 °C, the fluoride removal efficiency of calcium-impregnated silica combined with titanium dioxide increased. It started decreasing by increasing the accretion of fluoride on the surface of the adsorbent due to the attractive force amid fluoride ions [38]. According to a research study, sorption capacity increased with a temperature increase up to a certain level and then began to decrease with further temperature increases [39]. From the considered temperature (24.85-59.85 °C), the maximum fluoride removal was observed at 24.85 °C in a research study [40].

3.3.5 Response of initial ion concentration

In batch experiments with varying initial ion concentrations (2, 5, 8, 10, 13, and 15 mg/l), a 0.9 g dose at pH 2 and 120 min at 30 °C, nanocellulose adsorption capacity was observed. The maximum fluoride removal (74%) at 2 mg/l, 0.9 g dose, 120 min, and pH 2 was reduced to (65%) at 15 mg/l, as shown in Figure 4(e). The results showed that defluoridation reduced as ion concentration increased because the capacity of adsorbent material can exhaust abruptly due to an increase in fluoride ion concentration; similar results were observed on the rice husk adsorbent [35].

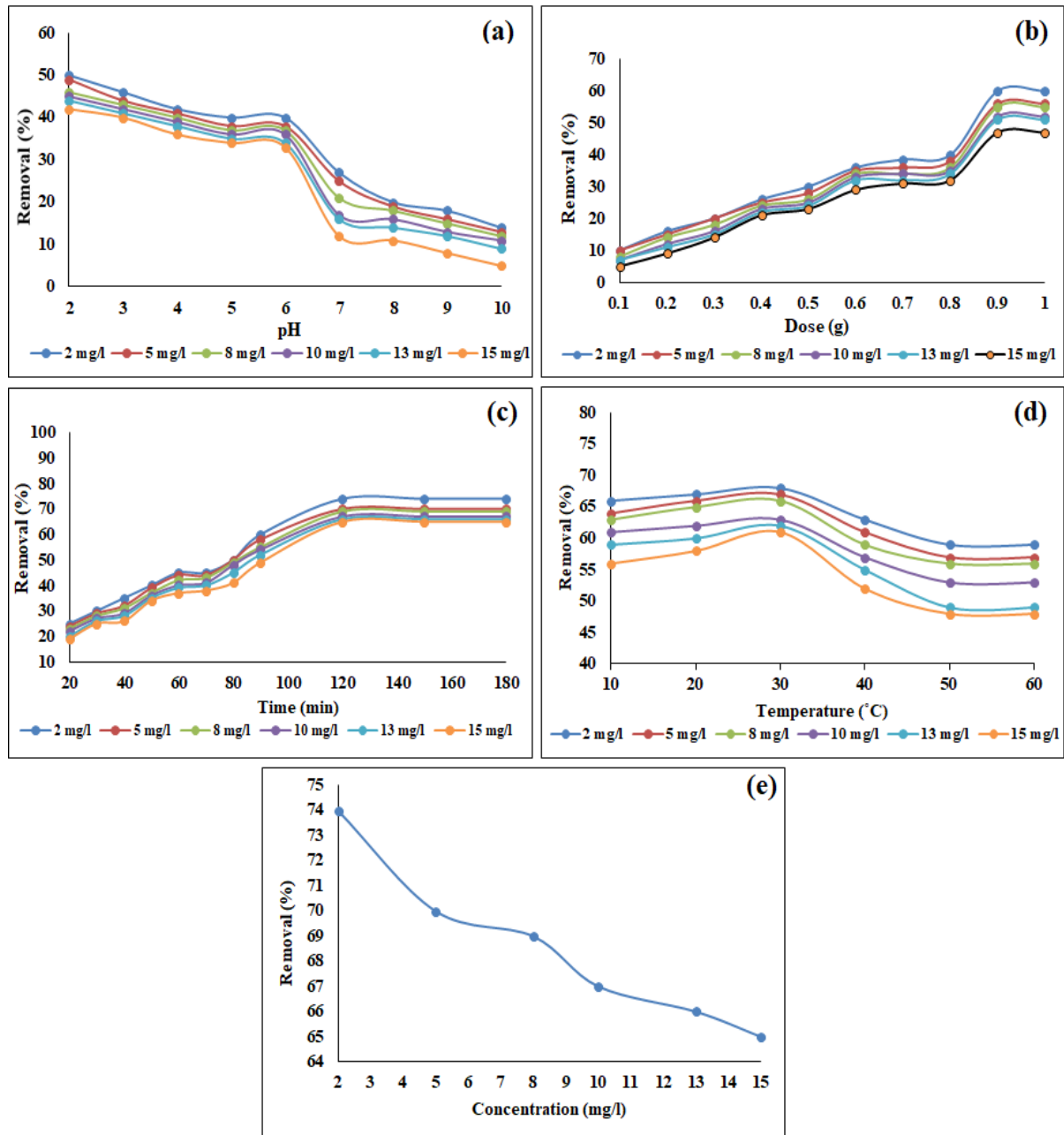


Fig.4. Response a) pH, b) Dose, c) Time, d) Temperature, and e) Initial ion concentration.

3.4. Adsorption kinetics

3.4.1 Pseudo-first-order and pseudo-second-order kinetic models

The process of adsorption and the latent rate-limiting phase is determined by kinetic models of adsorption. Both the pseudo-first-order and pseudo-second-order kinetic models were applied to analyze the adsorption process. The pseudo-first-order kinetic model in a linear form is expressed in Equation (9) [41]:

$$\ln q_t = \ln C_0 - k_1 t \quad (9)$$

Where, q_e and q_t (mg/g) are the solute amount at a steady-state time and time t (min), respectively, and k_1 is the rate constant (min^{-1}). The pseudo-second-order model in a linear form is expressed in Equation (10) [42,43].

$$\frac{t}{q_t} = \frac{1}{k_2 q_e^2} + \frac{1}{q_e} * t \quad (10)$$

Where, K_2 (g/mg/min) is the rate constant of the pseudo-second-order and q_t and q_e (mg/g) are the solute amounts at time t (min) and equilibrium, respectively.

The curvatures of the pseudo-first-order kinetic model and pseudo-second-order kinetic models are shown in Figures 5(a) and (b), respectively, and the parameter values described in Table 3. The correlation coefficient (R^2) of the pseudo-first-order kinetic model was lower, which demonstrated that the pseudo-first-order kinetic model did not explain the sorption. It is because the pseudo-first-order kinetic model was appropriate at an early phase [44]. So, it does not fit well with the entire process of adsorption. But, for the pseudo-second-order model, the R^2 value was high. As a result, the adsorption process fits with the pseudo-second-order kinetic model, which follows the whole adsorption process.

3.4.2. Intra-particle diffusion

The intra-particle diffusion model describes how species travel from the majority of the solution to

the solid phase. The rate constant can be determined by plotting the amount of sorbate sorbed, q_t (mg/g), and the square root of time (slope), as shown in Figure 5(c). The intercept values revealed the boundary layer thickness and as the intercept increased, external mass transfer resistance also increased. The linear form of the intra-particle diffusion model is expressed in Equation (11):

$$q_t = k_{id}t^{(1/2)} + C_i \quad (11)$$

where, K_{id} (mg/g/min^(1/2)) is the diffusion coefficient measure and C_i (mg/g) intra-particle diffusion constant. It is directly proportional to the boundary layer thickness. The correlation coefficient ($R^2=0.942$) showed that intra-particle diffusion fitted well with the adsorption process.

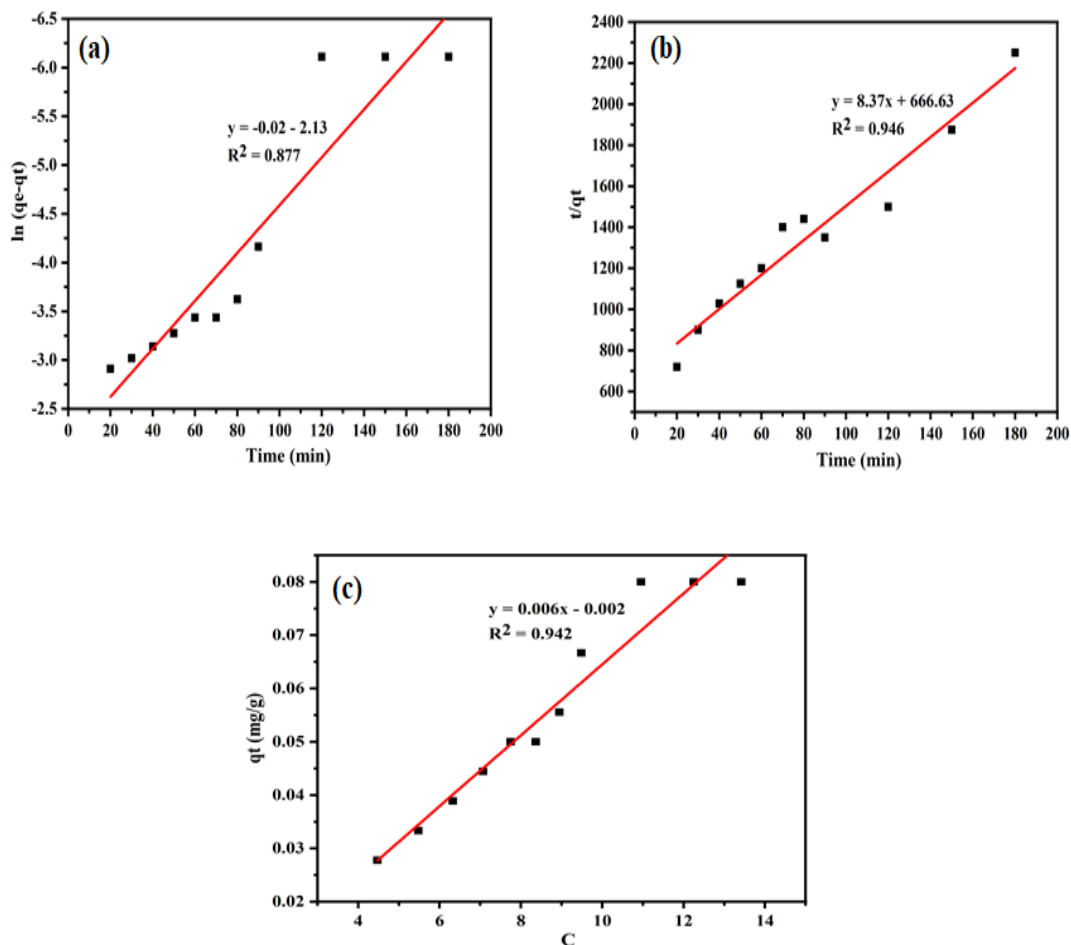


Fig.5. Kinetic models: a) Pseudo-first-order, b) Pseudo-second-order, and c) Intra-particle diffusion.

Table 3. Pseudo-First-Order and Pseudo-Second-Order Kinetic, and Intra-Particle Diffusion Model Constants.

Kinetic Model	Equation	Constant	Values
Pseudo-first-order	$\ln q_t = \ln C_0 - k_1 t$	q_e (mg/g)	0.118
		K_1	-0.0002
		R^2	0.877
Pseudo-second-order	$\frac{t}{q_t} = \frac{1}{k_2 q_e^2} + \frac{1}{q_e} * t$	q_e (mg/g)	0.119
		q_e^2	0.014
		K_2	0.105
		R^2	0.946
Intra-particle diffusion	$q_t = k_{id} t^{(1/2)} + C_i$	K_{id}	0.006
		C_i	-0.002
		R^2	0.942

3.5. Adsorption isotherms

3.5.1. Langmuir and Freundlich isotherm

Langmuir and Freundlich are two parameter adsorption isotherm models that demonstrate the connection between adsorbent and adsorbate. The Freundlich isotherm uses heterogeneous and multilayer sorption having active non-uniform distribution, whereas the Langmuir isotherms model uses a saturated molecular layer [45,46]. The Freundlich model in linear form is expressed in Equation (12):

$$\frac{t}{q_t} = \frac{1}{k_2 q_e^2} + \frac{1}{q_e} * t \quad (12)$$

where, fluoride equilibrium concentration is C_e (mg/l), equilibrium adsorption capacity is q_e (mg/g), and n and K_f (mg/g) are constants of heterogeneity factor and adsorption capacity, respectively. The Langmuir isotherm in linear form is expressed in Equation (13):

$$\frac{1}{Q_e} = \frac{1}{Q_{max}} \frac{1}{b C_e} + \frac{1}{Q_{max}} \quad (13)$$

where, fluoride solution equilibrium concentration is C_e (mg/l), the equilibrium capacity of adsorption is q_e (mg/g), the Langmuir constant is b (mg/l) associated with adsorption energy, and a max capacity of adsorption adsorbent is Q_{max} (mg/g) calculated as a constant of Langmuir isotherm. The Langmuir model determines R_L is the equilibrium parameter for dimensionless constant [47] can be stated in Equation (14) as:

$$R_L = \frac{1}{1 + b C_0} \quad (14)$$

where, the initial concentration of fluoride is C_0 (mg/l) and the Langmuir constant is b (mg/l). Freundlich and Langmuir isotherms for the adsorption of fluoride are illustrated in Figure 6 (a) and (b), and the parameter values are described in Table 4. For Langmuir and Freundlich isotherm models, the correlation coefficient (R^2) obtained was 0.99, and both models fitted well to the fluoride sorption process on nanocellulose. $1/n$ calculated is 0.819 ($1/n < 1$), showing increased bond energies with a density of the surface. The maximum adsorption capacity (Q_{max}) is 1.148 mg/g. The results reveal that nanocellulose played a vital role in fluoride adsorption.

3.5.2. Temkin isotherm

Temkin is a two-parameter isotherm model that depicts the interface between sorbents and adsorbed organic molecules [48]. The linear form of Temkin isotherm in Equation (15) is stated as:

$$q_e = B \ln A + B \ln C_e \quad (15)$$

where, C_e is the adsorbate concentration at steady state (mg/l), q_e is the quantity of adsorbate adsorbed at steady state (mg/g), and $K_T/B_T = B$, whereas K_T and B_T are constants. The linear plot between q_e versus $\ln C_e$, as shown in Figure 6(c), was used for the calculation of B_T and K_T constants. The constant (B_T) is associated with the heat of adsorption and the binding constant equilibrium (K_T), which is equivalent to the maximum binding energy. B_T and K_T values are described in Table 4. The B_T value was (0.195 kJ/mol) and specified that the interface between the fluoride and nanocellulose was sturdy. The R^2 -0.918 demonstrated that the Temkin model fitted well

with the adsorption process of fluoride on nanocellulose.

3.5.3. Redlich-Peterson isotherm

The Langmuir and Freundlich isotherms are combined in the Redlich-Peterson (R-P) model; it is a three-parameter hybrid adsorption model that describes homogeneous and heterogeneous adsorption with the values of n characterized by the adsorption behaviour. In this model, sorbate adsorbs on the adsorbent in both mono and multilayer (hybrid adsorption) [49].

The R-P isotherm's non-linear expression is given in Equation (16):

$$N \text{ or } q_e = \frac{K C_e}{[1 + a(C_e)^n]} \quad (16)$$

where, N is the amount adsorbed at equilibrium, a is the Redlich-Peterson adsorption capacity constant, K is the Redlich-Peterson constant, and n is an exponent between 0 and 1. The Redlich-Peterson isotherm is more accurate than the Langmuir and Freundlich isotherms because it is a three-parameter model, with the Langmuir and Freundlich isotherms emerging from the Redlich-Peterson isotherm [50-55]. The Redlich-Peterson equation changes into the Langmuir isotherm equation when $n=1$ and is close to the Freundlich equation when $n=0$ [56-59]. The non-linear plot between N versus C_e , as shown in Figure 6(d), was used for the calculation of the constants. K , n , and a value are described in Table 4. The n value was 0.42 and specified that it was near to the Freundlich isotherm equation. The correlation coefficient ($R^2=0.998$) demonstrated that the Redlich-Peterson isotherm model fitted well in the adsorption process of fluoride on nanocellulose.

3.5.4. Baudu isotherm

Baudu is a four-parameter isotherm model that determines the assessment of the Langmuir constants, b and Q_{max} , by the extent of tangents at varied equilibrium concentrations, demonstrating that they are not constants in a wider array [60]; hence, the Langmuir isotherm has been modified to the Baudu isotherm [61]. The non-linear Baudu isotherm is expressed in Equation (17):

$$q_e = \frac{q_m b_0 C_e^{1+x+y}}{1 + b_0 C_e^{1+x}} \quad (17)$$

where, q_m (mg/g) is the maximum capacity of adsorption, b_0 is the equilibrium constant, and x and y are Baudu constraints. Because of innate bias resulting from linearization, Baudu isotherm constraints are analyzed by the non-linear regression method [62]. It is reduced to the Freundlich equation with smaller coverage of the surface. The values for q_m , b_0 , x , and y were calculated using the non-linear plot between q_e and C_e depicted in Figure 6(e) and are presented in Table 4. The maximum adsorption capacity of nanocellulose reported the Baudu adsorption isotherm as 1.41 mg/g. The correlation coefficient ($R^2=0.998$) demonstrated that the Baudu isotherm model fitted well in the adsorption process of fluoride on nanocellulose.

3.6. Thermodynamics and activation energy

Because of the practicability of the sorption process, thermodynamic constraints, such as enthalpy (ΔH°), Gibb's free energy (ΔG°), and entropy (ΔS°) variations, were observed using following equation (18) [63]:

$$\ln K_L = \frac{\Delta S^\circ}{R} - \frac{\Delta H^\circ}{RT} \quad (18)$$

Where, K_L is the distribution adsorbent coefficient that was determined by q_e/C_e , T is the temperature (K) of the solution, and gas constant R (8.314 J/mol/K). From the slope and intercept of the plot ($\ln K_L$ v/s $1/T$), ΔH° and ΔS° were computed. ΔG° can be computed by using Equation (19) [64]:

$$\Delta G^\circ = -RT \ln K_L \quad (19)$$

The Arrhenius equation (20) was used to determine the adsorption activation energy:

$$\ln K_1 = \ln A - \frac{E_a}{RT} \quad (20)$$

where, k_1 is the rate constant of adsorption, activation energy is E_a (kJ/mol), the gas constant is R (8.314 J/mol/K), Arrhenius constant is (A), and Temperature is (T). The thermodynamic parameters are described in Table 5. By plotting $\ln K_L$ v/s $1/T$ (Figure 7), E_a was attained using the Arrhenius equation. As a result of the negative values of ΔG° at studied temperatures, the reaction was impulsive. By increasing the temperature, the value of ΔG° also increased, indicating that adsorption occurred at lower temperatures. ΔG° ranged from 0 to 20 kJ/mol for physical adsorption and from 80 to 400 kJ/mol for chemical sorption

[65]. In this study, the ΔG° value varied from -5.59 to -6.22 kJ/mol, demonstrating that adsorption occurred physically. The positive value of ΔH° (3.22 kJ/mol) indicates endothermic adsorption. The magnitude of ΔH° can be used to characterize the nature of adsorption. Physical sorption produces heat in the range of 2.1-20.9 kJ/mol, whereas chemical sorption produces heat in the range of 80-200 kJ/mol [66]. The sorption of nanocellulose can be ascribed to the physical adsorption process.

The present study showed that the positive value of ΔS° (31.14 JK/mol) indicated it was enthalpy determined. Using the Arrhenius equation, the calculated E_a value was 1.66, kJ/mol, described in Table 5. The E_a positive value indicated that a higher solution temperature favours fluoride removal through adsorption on nanocellulose and showed that the adsorption process was endothermic.

Table 4. Freundlich, Langmuir, Temkin, Redlich-Peterson, and Baudu Isotherm constants.

Isotherm Model	Equation	Constant	Values
Freundlich (Two parameters)	$\frac{t}{q_t} = \frac{1}{k_2 q_e^2} + \frac{1}{q_e} * t$	1/n	0.819
		K_f	0.14
		R^2	0.999
Langmuir (Two parameters)	$\frac{1}{Q_e} = \frac{1}{Q_{\max}} \frac{1}{b C_e} + \frac{1}{Q_{\max}}$ $R_L = \frac{1}{1 + b C_0}$	Q_{\max}	1.148
		b	0.147
		R_L	0.772
		R^2	0.997
Temkin (Two parameters)	$q_e = B \ln A + B \ln C_e$	B_T	0.195
		K_T	2.343
		R^2	0.918
Redlich-Peterson (Three parameters)	$N \text{ or } q_e = \frac{K C_e}{[1 + a(C_e)^n]}$	a	0.55
		n	0.42
		K	0.22
		R^2	0.998
Baudu (Four parameters)	$q_e = \frac{q_m b_0 C_e^{1+x+y}}{1 + b_0 C_e^{1+x}}$	Q_m	1.41
		b_0	1.276
		x	0.276
		y	-0.422
		R^2	0.998

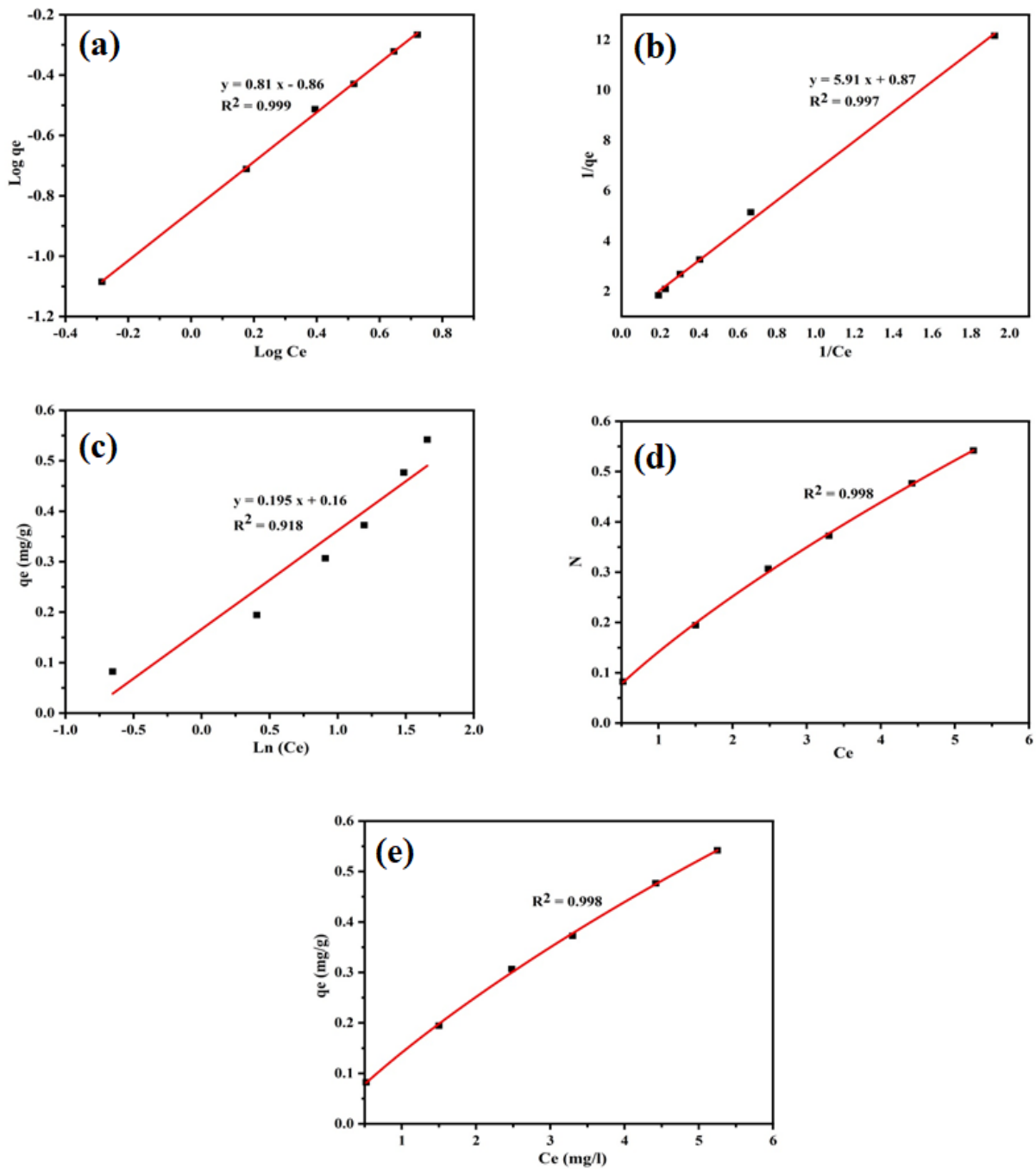


Fig.6. Isotherm models: a) Freundlich, b) Langmuir, c) Temkin, d) Redlich-Peterson, and e) Baudu.

Table 5. Thermodynamic parameters.

Temperature (K)	K_L	$\text{Ln } K_L$	ΔG° (KJ/mol)	ΔH° (KJ/mol)	ΔS° (JK/mol)	E_a (KJ/mol)	R^2
283.15	10.78	2.37	-5.59				
293.15	11.27	2.42	-5.90	3.22	31.14	1.66	0.998
303.15	11.8	2.46	-6.22				

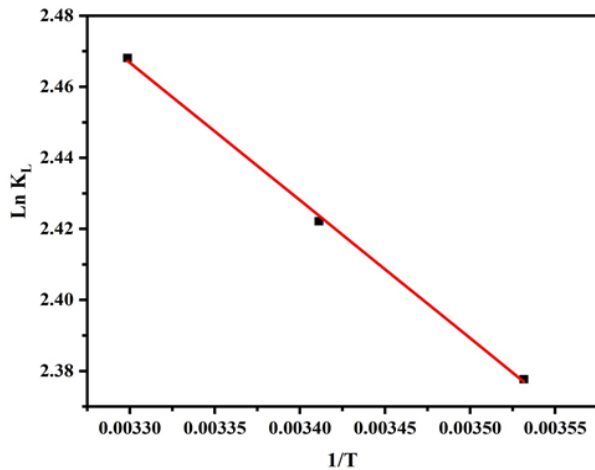


Fig.7. Thermodynamic plot for fluoride removal using nanocellulose.

3.7. Adsorption capacity

The amount of adsorbate absorbed per unit mass (or volume) of the adsorbent is the adsorption capacity. The adsorption capacity (mg/g) for fluoride removal using different adsorbents in various research studies is described in Table 6. Adsorption capacity depends on the sorbent used and pH conditions. Sorbent includes agriculturally based, modified adsorbents, ashes, etc. In the present study, the nanocellulose using rice husk had a 1.41 mg/g adsorption capacity. Banana peel adsorbent (0.479 mg/g) has the minimum adsorption capacity, and ionic liquid-modified chitosan (8.06%) has the maximum adsorption capacity, described in Table 6.

3.8. Regeneration study

The batch study showed a maximum of 74% defluoridation using the nanocellulose under

Table 6. Adsorption capacity of fluoride removal using different adsorbent.

Adsorbent	pH	Maximum Adsorption Capacity (mg/g)	References
Ionic liquid-modified chitosan	4.0	8.06	[67]
Activated Carbon of Avocado Seeds	6.6	1.20	[68]
Rice Husk Ash	8.0	2.90	[69]
Sugarcane Bagasse	5.4	2.44	[70]
Banana Peel	5.0	0.48	[71]
Sawdust	7.0	16.50	[72]
Coconut Husk Activated Carbon	5.0	6.50	[73]
Nanocellulose using Rice Husk	2.0	1.41	Present Study

optimum conditions, and regeneration studies were conducted to confirm the bond strength between the adsorbent and adsorbate. Five desorption cycles were carried out using NaOH (0.1-0.7M) for treating the sorbent after every cycle. 0.5M NaOH treated sorbent showed maximum defluoridation after each cycle without degradation of the sorbent. As cycles succeeded, defluoridation also decreased due to the unavailability of sites on the sorbent surface, as shown in Figure 8. Removal of fluoride by the 0.5M NaOH treated adsorbent was 67%, 54%, 28%, 11%, and 6% in the first, second, third, fourth, and fifth reuse cycles, respectively. The result indicated that sorbent reusability was economical and effective for up to two cycles. Economically and environmentally, regeneration is a crucial aspect of adsorption research. The disposal of used adsorbents is one of the biggest issues in the adsorption process. Regeneration can reduce the need for new adsorbents and ease the problem of discarding used ones.

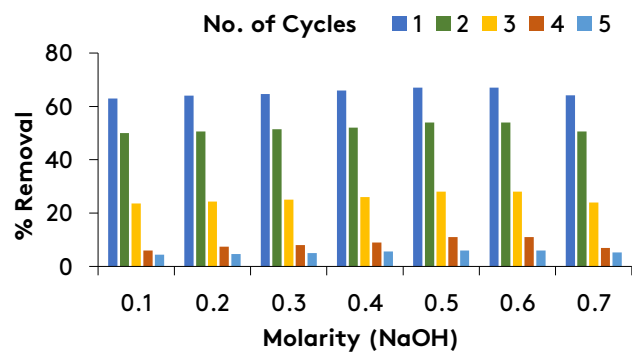


Fig.8. Regeneration study of nanocellulose.

4. Conclusions

The synthesized nanocellulose was characterized for functional groups (at peaks 1442 and 1641 cm^{-1}), morphology (spherical shape), crystalline structure (crystallinity Index of 70%), and particle height (5.7 nm) to confirm cellulose. A batch study was performed for defluoridation from an aqueous solution by nanocellulose. The highest defluoridation efficacy of nanocellulose was 74% at pH 2. The defluoridation decreased with an increase in the initial concentration of fluoride ions and pH, while it increased with an increase in adsorbent dosage and contact time to some extent after it reached equilibrium. The effect of temperature on adsorption revealed that fluoride removal percentage increased up to 30° C, then began to decline and reached equilibrium upon further temperature increase. Adsorption data fitted well with the tested isotherms. The maximum adsorption capacity was 1.41 mg/g. Pseudo-second-order kinetic and intra-particle diffusion models fitted well with the adsorption data. The calculated value of activation energy was 1.66 KJ/mol. Fluoride removal was impulsive and endothermic, and adsorption increased due to distraction at the solution interface. The regeneration study showed that sorbent reuse was cost-effective and efficient for two cycles.

References

- [1] Vijila, B., Gladis, E. E., Jose, J. M. A., Sharmila, T. M., Joseph, J. (2021). Removal of fluoride with rice husk derived adsorbent from agro waste materials. *Materials Today: Proceedings*, 45, 2125-2129.
<http://doi.org/10.1016/j.matpr.2020.09.729>
- [2] Meenakshi, Garg, V. K., Kavita, Renuka, Malik, A. (2004). Groundwater quality in some villages of Haryana, India: focus on fluoride and fluorosis. *Journal of Hazardous Materials*, 106(1), 85-97.
<http://doi.org/10.1016/j.jhazmat.2003.09.007>
- [3] World Health Organization (2001). Environmental Health Criteria (EHC).
- [4] Jolly, S.S., Sing, B.M., Mathur, O.C. (1969). Endemic fluorosis in Punjab (India). *The American Journal of Medicine*, 47(4), 553-563.
[https://doi.org/10.1016/0002-9343\(69\)90186-7](https://doi.org/10.1016/0002-9343(69)90186-7)
- [5] Oguz, E. (2005). Adsorption of fluoride on gas concrete materials. *Journal of Hazardous Materials*, 117(2-3), 227-233.
<https://doi.org/10.1016/j.jhazmat.2004.09.020>
- [6] Dehbandi, R., Moore, F., Keshavarzi, B. (2018). Geochemical sources, hydrogeochemical behavior, and health risk assessment of fluoride in an endemic fluorosis area, central Iran. *Chemosphere*, 193, 763-776.
<https://doi.org/10.1016/j.chemosphere.2017.11.021>
- [7] Mukherjee, I., Singh, U.K., Patra, P.K. (2019). Exploring a multi-exposure-pathway approach to assess human health risk associated with groundwater fluoride exposure in the semi-arid region of east India. *Chemosphere*, 233, 164-173.
<https://doi.org/10.1016/j.chemosphere.2019.05.278>
- [8] Miretzky, P. and Cirelli, A.F. (2011). Fluoride removal from water by chitosan derivatives and composites: a review. *Journal of Fluorine Chemistry*, 132(4), 231-240.
<https://doi.org/10.1016/j.jfluchem.2011.02.001>
- [9] Lahnid, S., Tahaikt, M., Elaroui, K., Idrissi, I., Hafsi, M., Laaziz, I. (2008). Economic evaluation of fluoride removal by electrodialysis. *Desalination*, 230(1-3), 213-219.
<https://doi.org/10.1016/j.desal.2007.11.027>
- [10] Reardon, E.J. and Wang, Y. X. (2000). A limestone reactor for fluoride removal from wastewaters. *Environmental Science and Technology*, 34(15), 3247-3253.
<https://doi.org/10.1021/es990542k>
- [11] Ndiayea, P.I., Moulin, P., Dominguez, L., Millet, J.C., Charbit, F. (2005). Removal of fluoride from electronic industrial effluent by RO membrane separation. *Desalination*, 173(1), 25-32.
<https://doi.org/10.1016/j.desal.2004.07.042>
- [12] Meenakshi, S. and Viswanathan, N. (2007). Identification of selective ion-exchange resin for fluoride sorption. *Journal of Colloid and Interface Science*, 308(2), 438-450.
<https://doi.org/10.1016/j.jcis.2006.12.032>
- [13] Ahmed, S.A. (2011). Batch and fixed-bed column techniques for removal of Cu (II) and Fe (III) using carbohydrate natural polymer

- modified complexing agents. *Carbohydrate Polymers*, 83(4), 1470-1478.
<http://dx.doi.org/10.1016/j.carbpol.2010.09.051>
- [14] Akafu, T., Chimdi, A., Gomoro, K. (2019). Removal of fluoride from drinking water by sorption using diatomite modified with aluminum hydroxide. *Journal of analytical methods in chemistry*, 2019.
<https://doi.org/10.1155/2019/4831926>
- [15] Waghmare, S., Arfin, T., Rayalu, S., Lataye, D., Dubey, S., Tiwari, S. (2015). Adsorption behavior of modified zeolite as novel adsorbents for fluoride removal from drinking water: surface phenomena, kinetics and thermodynamics studies. *International Journal of Science, Engineering and Technology Research*, 4(12), 4114-4124.
- [16] Bhatnagar, A., Kumar, E., Sillanpaa, M. (2011). Fluoride removal from water by adsorption—a review. *Chemical Engineering Journal*, 171(3), 811-840.
<https://doi.org/10.1016/j.cej.2011.05.028>
- [17] Mohapatra, M., Anand, S., Mishra, B.K., Giles, D.E., Singh, P. (2009). Review of fluoride removal from drinking water. *Journal of Environmental Management*, 91(1), 67-77.
<https://doi.org/10.1016/j.jenvman.2009.08.015>
- [18] Yu, X., Tong, S., Ge, M., Zuo, J. (2013). Removal of fluoride from drinking water by cellulose @ hydroxyapatite nanocomposites. *Carbohydrate Polymers*, 92(1), 269-275.
<https://doi.org/10.1016/j.carbpol.2012.09.045>
- [19] Han, R., Wang, Y., Yu, W., Zou, W., Shi, J., Liu, H. (2007). Biosorption of methylene blue from aqueous solution by rice husk in a fixed-bed column. *Journal of Hazardous Materials*, 141(3), 713-718.
<https://doi.org/10.1016/j.jhazmat.2006.07.031>
- [20] Vardhan, C. V., Karthikeyan, J. (2011, September). Removal of fluoride from water using low-cost materials. In *Fifteenth International Water Technology Conference, IWTC-15* (Vol. 1, No. 2, pp. 1-14).
- [21] Goering, H. K., Van Soest, P. J. (1970). *Forage fiber analyses (apparatus, reagents, procedures, and some applications)* (No. 379). US Agricultural Research Service.
<https://doi.org/10.4236/fns.2013.48105>
- [22] Ananthi, A., Geetha, D., Ramesh, P.S. (2016). Preparation and characterization of silica material from rice husk ash—an economically viable method. *Chemistry and Materials Research*, 8(6), 1-7.
- [23] Ma'ruf, A., Pramudono, B., Aryanti, N. (2017, March). Lignin isolation process from rice husk by alkaline hydrogen peroxide: Lignin and silica extracted. In *AIP Conference Proceedings* (Vol. 1823, No. 1). AIP Publishing.
<https://doi.org/10.1063/1.4978086>
- [24] Chandra, J., George, N., Narayanankutty, S.K. (2016). Isolation and characterization of cellulose nanofibrils from arecanut husk fibre. *Carbohydrate Polymers*, 142, 158-166.
<https://doi.org/10.1016/j.carbpol.2016.01.015>
- [25] Mandal, A. and Chakrabarty, D. (2011). Isolation of nanocellulose from waste sugarcane bagasse (SCB) and its characterization. *Carbohydrate Polymers*, 86(3), 1291-1299.
<https://doi.org/10.1016/j.carbpol.2011.06.030>
- [26] Alemdar, A. and Sain, M. (2008). Biocomposites from wheat straw nanofibres: Morphology, thermal and mechanical properties. *Composites Science and Technology*, 68(2), 557-565.
<https://doi.org/10.1016/j.compscitech.2007.05.044>
- [27] Segal, L.G.J.M.A., Creely, J.J., Martin Jr, A.E., Conrad, C.M. (1959). An empirical method for estimating the degree of crystallinity of native cellulose using the X-ray diffractometer. *Textile Research Journal*, 29(10), 786-794.
<https://doi.org/10.1177/004051755902901003>
- [28] de Souza Lima, M.M. and Borsali, R. (2004). Rodlike cellulose microcrystals: structure, properties, and applications. *Macromolecular Rapid Communications*, 25(7), 771-787.
<https://doi.org/10.1002/marc.200300268>
- [29] Tang, L.G., Hon, D.N.S., Pan, S.H., Zhu, Y.Q., Wang, Z., Wang, Z.Z. (1996). Evaluation of microcrystalline cellulose. I. Changes in ultrastructural characteristics during preliminary acid hydrolysis. *Journal of Applied Polymer Science*, 59(3), 483-488.
[https://doi.org/10.1002/\(SICI\)1097-4628\(19960118\)59:3<483::AID-APP13>3.0.CO;2-V](https://doi.org/10.1002/(SICI)1097-4628(19960118)59:3<483::AID-APP13>3.0.CO;2-V)

- [30] Azizi Samir, M.A.S., Alloin, F., Dufresne, A. (2005). Review of recent research into cellulosic whiskers, their properties and their application in nanocomposite field. *Biomacromolecules*, 6(2), 612-626.
<https://doi.org/10.1021/bm0493685>
- [31] Moran, J.I., Alvarez, V.A., Cyras, V.P., Vázquez, A. (2008). Extraction of cellulose and preparation of nanocellulose from sisal fibres. *Cellulose*, 15(1), 149-159.
<https://doi.org/10.1007/s10570-007-9145-9>
- [32] Silverio, H.A., Neto, W.P.F., Dantas, N.O., Pasquini, D. (2013). Extraction and characterization of cellulose nanocrystals from corncob for application as reinforcing agent in nanocomposites. *Industrial Crops and Products* 44, 427-436.
<https://doi.org/10.1016/j.indcrop.2012.10.014>
- [33] Johar, N., Ahmad, I., Dufresne, A. (2012). Extraction, preparation and characterization of cellulose fibres and nanocrystals from rice husk. *Industrial Crops and Products*, 37(1), 93-99.
<https://doi.org/10.1016/j.indcrop.2011.12.016>
- [34] Hornsby, P.R., Hinrichsen, E., Tarverdi, K. (1997). Preparation and properties of polypropylene composites reinforced with wheat and flax straw fibres: part I fibre characterization. *Journal of Materials Science*, 32(2), 443-449.
<https://doi.org/10.1023/A:1018521920738>
- [35] Deshmukh, W.S., Attar, S.J., Waghmare, M.D. (2009). Investigation on fluoride in water using rice husk as an adsorbent. *Nature, Environment and Pollution Technology*, 8(2), 217-223.
- [36] Tembhurkar, A.R. and Dongre, S. (2006). Studies on fluoride removal using adsorption process. *Journal of Environmental Science and Engineering*, 48(3), 151-156.
- [37] Yadav, A.K., Kaushik, C.P., Haritash, A.K., Kansal, A., Rani, N. (2006). Defluoridation of groundwater using brick powder as an adsorbent. *Journal of Hazardous materials*, 128(2-3), 289-293.
<https://doi.org/10.1016/j.jhazmat.2005.08.006>
- [38] Roy, S., Das, P., Sengupta, S. (2017). Thermodynamics and kinetics study of defluoridation using Ca-SiO₂-TiO₂ as adsorbent: column studies and statistical approach. *Korean Journal of Chemical Engineering*, 34(1), 179-188.
<https://doi.org/10.1007/s11814-016-0217-0>
- [39] Uddin, M.K., Ahmed, S.S., Naushad, M. (2019). A mini update on fluoride adsorption from aqueous medium using clay materials. *Desalination and Water Treatment*, 145, 232-248.
<https://doi.org/10.5004/dwt.2019.23509>
- [40] Kir, E., Oruc, H., Kir, I., Sardohan-Koseoglu, T. (2016). Removal of fluoride from aqueous solution by natural and acid-activated diatomite and ignimbrite materials. *Desalination and Water Treatment*, 57(46), 21944-21956.
<https://doi.org/10.1080/19443994.2015.1124346>
- [41] Jamode, A.V., Sapkal, V.S., Jamode, V.S., Deshmukh, S.K. (2004). Adsorption kinetics of defluoridation using low-cost adsorbents. *Adsorption Science and Technology*, 22(1), 65-73.
<https://doi.org/10.1260/026361704323151>
- [42] Chandra, V., Park, J., Chun, Y., Lee, J.W., Hwang, I.C., Kim, K.S. (2010). Water-dispersible magnetite-reduced graphene oxide composites for arsenic removal. *ACS nano*, 4(7), 3979-3986.
<https://doi.org/10.1021/nn1008897>
- [43] Ho, Y.S. and McKay, G. (1999). Pseudo-second order model for sorption processes. *Process Biochemistry*, 34(5), 451-465.
[https://doi.org/10.1016/S0032-9592\(98\)00112-5](https://doi.org/10.1016/S0032-9592(98)00112-5)
- [44] Ho, Y.S. and McKay, G. (1999). The sorption of lead (II) ions on peat. *Water Research*, 33(2), 578-584.
[https://doi.org/10.1016/S0043-1354\(98\)00207-3](https://doi.org/10.1016/S0043-1354(98)00207-3)
- [45] Freundlich, H. (1906). Concerning adsorption in solutions. *Zeitschrift Fur Physikalische Chemie—Stoichiometrie Und Verwandtschaftslehre*, 57(4), 385-470.
- [46] Langmuir, I. (1918). Adsorption of gases on plain surfaces of glass, mica platinum. *Journal of the American Chemical Society*, 40, 1361-1403.
<https://doi.org/10.1021/ja02242a004>

- [47] Tian, Y., Wu, M., Lin, X., Huang, P., Huang, Y. (2011). Synthesis of magnetic wheat straw for arsenic adsorption. *Journal of Hazardous Materials*, 193, 10-16.
<https://doi.org/10.1016/j.jhazmat.2011.04.093>
- [48] Chen, Z., Ma, W., Han, M. (2008). Biosorption of nickel and copper onto treated alga (*Undariapinnatifida*): application of isotherm and kinetic models. *Journal of Hazardous Materials*, 155(1-2), 327-333.
<https://doi.org/10.1016/j.jhazmat.2007.11.064>
- [49] Foo, K.Y. and Hameed, B.H. (2010). Insights into the modeling of adsorption isotherm systems. *Chemical Engineering Journal*, 156(1), 2-10.
<https://doi.org/10.1016/j.cej.2009.09.013>
- [50] Benhammou, A., Yaacoubi, A., Nibou, L., Tanouti, B. (2005). Adsorption of metal ions onto Moroccan stevensite: kinetic and isotherm studies. *Journal of Colloid and Interface Science*, 282(2), 320-326.
<https://doi.org/10.1016/j.jcis.2004.08.168>
- [51] Srivastava, V.C., Swamy, M.M., Mall, I.D., Prasad, B., Mishra, I.M. (2006). Adsorptive removal of phenol by bagasse fly ash and activated carbon: equilibrium, kinetics and thermodynamics. *Colloids and Surfaces a: Physicochemical and Engineering Aspects*, 272(1-2), 89-104.
<https://doi.org/10.1016/j.colsurfa.2005.07.016>
- [52] Allen, S.J., McKay, G., Porter, J.F. (2004). Adsorption isotherm models for basic dye adsorption by peat in single and binary component systems. *Journal of Colloid and Interface Science*, 280(2), 322-333.
<https://doi.org/10.1016/j.jcis.2004.08.078>
- [53] Tsai, W.T., Hsu, H.C., Su, T.Y., Lin, K.Y., Lin, C.M. (2006). Adsorption characteristics of bisphenol-A in aqueous solutions onto hydrophobic zeolite. *Journal of Colloid and Interface Science*, 299(2), 513-519.
<https://doi.org/10.1016/j.jcis.2006.02.034>
- [54] Artola, A., Martin, M., Balaguer, M., Rigola, M. (2000). Isotherm model analysis for the adsorption of Cd (II), Cu (II), Ni (II), and Zn (II) on anaerobically digested sludge. *Journal of Colloid and Interface Science*, 232(1), 64-70.
<https://doi.org/10.1006/jcis.2000.7186>
- [55] Wu, F.C., Liu, B.L., Wu, K.T., Tseng, R. L. (2010). A new linear form analysis of Redlich-Peterson isotherm equation for the adsorptions of dyes. *Chemical Engineering Journal*, 162(1), 21-27.
<https://doi.org/10.1016/j.cej.2010.03.006>
- [56] Wang, J.P., Feng, H.M., Yu, H.Q. (2007). Analysis of adsorption characteristics of 2, 4-dichlorophenol from aqueous solutions by activated carbon fibre. *Journal of Hazardous Materials*, 144(1-2), 200-207.
<https://doi.org/10.1016/j.jhazmat.2006.10.003>
- [57] Tor, A. and Cengeloglu, Y. (2006). Removal of congo red from aqueous solution by adsorption onto acid activated red mud. *Journal of Hazardous Materials*, 138(2), 409-415.
<https://doi.org/10.1016/j.jhazmat.2006.04.063>
- [58] Kundu, S. and Gupta, A.K. (2007). Adsorption characteristics of As (III) from aqueous solution on iron oxide coated cement (IOCC). *Journal of Hazardous Materials*, 142(1-2), 97-104.
<https://doi.org/10.1016/j.jhazmat.2006.07.059>
- [59] Ozer, A. and Dursun, G. (2007). Removal of methylene blue from aqueous solution by dehydrated wheat bran carbon. *Journal of Hazardous Materials*, 146(1-2), 262-269.
<https://doi.org/10.1016/j.jhazmat.2006.12.016>
- [60] McKay, G., Mesdaghinia, A., Nasser, S., Hadi, M., Aminabad, M.S. (2014). Optimum isotherms of dyes sorption by activated carbon: Fractional theoretical capacity and error analysis. *Chemical Engineering Journal*, 251, 236-247.
<https://doi.org/10.1016/j.cej.2014.04.054>
- [61] Ravnote, O.M. and Adsorpcizo, N.I.Z. (2013). Evaluation of equilibrium isotherm models for the adsorption of Cu and Ni from wastewater on bentonite clay. *Materiali in Tehnologije*, 47(4), 481-486.
- [62] Van Vliet, B.M., Weber Jr, W.J., Hozumi, H. (1980). Modeling and prediction of specific compound adsorption by activated carbon and synthetic adsorbents. *Water Research* 14(12), 1719-1728.
[https://doi.org/10.1016/0043-1354\(80\)90107-4](https://doi.org/10.1016/0043-1354(80)90107-4)
- [63] Hamad, B.K., Noor, A.M., Rahim, A.A. (2011). Removal of 4-chloro-2-methoxyphenol from aqueous solution by adsorption to oil palm shell

- activated carbon activated with K_2CO_3 . *Journal of Physical Science*, 22(1), 39-55.
- [64] Sujana, M.G., Pradhan, H.K., Anand, S. (2009). Studies on sorption of some geomaterials for fluoride removal from aqueous solutions. *Journal of Hazardous Materials*, 161(1), 120-125.
<https://doi.org/10.1016/j.jhazmat.2008.03.062>
- [65] Yu, Y., Zhuang, Y.Y., Wang, Z.H., Qiu, M.Q. (2004). Adsorption of water-soluble dyes onto modified resin. *Chemosphere*, 54(3), 425-430.
[https://doi.org/10.1016/S0045-6535\(03\)00654-4](https://doi.org/10.1016/S0045-6535(03)00654-4)
- [66] Liu, Y. and Liu, Y.J. (2008). Biosorption isotherms, kinetics and thermodynamics. *Separation and Purification Technology*, 61(3), 229-242.
<https://doi.org/10.1016/j.seppur.2007.10.002>
- [67] Dzieniszewska, A., Nowicki, J., Rzepa, G., Kyziol-Komosinska, J., Semeniuk, I., Kiełkiewicz, D., Czupioł, J. (2022). Adsorptive removal of fluoride using ionic liquid-functionalized chitosan—Equilibrium and mechanism studies. *International Journal of Biological Macromolecules*, 210, 483-493.
<https://doi.org/10.1016/j.ijbiomac.2022.04.179>
- [68] Tefera, N., Mulualem, Y., Fito, J. (2020). Adsorption of fluoride from aqueous solution and groundwater onto activated carbon of avocado seeds. *Water Conservation Science and Engineering*, 5(3), 187-197.
<https://doi.org/10.1007/s41101-020-00093-7>
- [69] Bibi, S., Farooqi, A., Yasmin, A., Kamran, M. A., Niazi, N. K. (2017). Arsenic and fluoride removal by potato peel and rice husk (PPRH) ash in aqueous environments. *International journal of Phytoremediation*, 19(11), 1029-1036.
<https://doi.org/10.1080/15226514.2017.1319329>
- [70] Singh, K., Lataye, D.H., Wastewater, K.L. (2016). Removal of fluoride from aqueous solution by using low-cost sugarcane bagasse: kinetic study and equilibrium isotherm analyses. *Journal of Hazardous, Toxic, and Radioactive Waste*, 20(3), 04015024.
[https://doi.org/10.1061/\(ASCE\)HZ.2153-5515.0000309](https://doi.org/10.1061/(ASCE)HZ.2153-5515.0000309)
- [71] Mondal, N.K. and Roy, A. (2018). Potentiality of a fruit peel (banana peel) toward abatement of fluoride from synthetic and underground water samples collected from fluoride affected villages of Birbhum district. *Applied Water Science*, 8(3), 1-10.
<https://doi.org/10.1007/s13201-018-0729-3>
- [72] Singh, N.B., Srivastava, Y.K., Shukla, S.P. (2019). Investigating the efficacy of saw dust in fluoride removal through adsorption. *Journal of The Institution of Engineers (India): Series A*, 100(4), 667-674.
<https://doi.org/10.1007/s40030-019-00387-7>
- [73] Talat, M., Mohan, S., Dixit, V., Singh, D.K., Hasan, S.H., Srivastava, O.N. (2018). Effective removal of fluoride from water by coconut husk activated carbon in fixed bed column: Experimental and breakthrough curves analysis. *Groundwater for Sustainable Development*, 7, 48-55.
<https://doi.org/10.1016/j.gsd.2018.03.001>